Reactively Steered Adaptive Array Using Microstrip Patch Elements at 4 GHz

ROBERT J. DINGER

Abstract—**A reactively steered adaptive array (RESAA) has one element connected by a transmission line to a receiver and a number of closely spaced parasitic elements, each of which is terminated by an adjustable reactive load. The pattern is formed by control of the reactive loads. Experimental results and the theory are presented for a RESAA consisting of five microstrip rectangular patch elements resonant at 4.0 GHz. Using steepest descent control of the reactive loads in a power inversion mode (no reference), we find that a null with a depth of 30 dB (relative to the pattern maximum) and an angular width of about 25° can be steered towards an interferer. Typically, about 40 steps (iterations) are needed for forming the null. With the slow power meter and general purpose minicomputer that served as the controller, adaptation times of several seconds are required; extrapolation to a dedicated microprocessor controller predicts adaptation times of several milliseconds. Operation in a mode using a reference signal demonstrates that the pattern can be shaped to steer a null toward interference and a lobe towards a desired signal. The nulling bandwidth is approximately 40 MHz with this array. The advantages of a RESAA, as compared with a conventional adaptive array, include the elimination of the mixers and other hardware needed to perform the complex weighting of the output of each element at an intermediate frequency, and better pattern control for closely spaced elements. These advantages are obtained at the expense of a more complicated control algorithm.**

I. INTRODUCTION

AN ESSENTIAL requirement for many communication and radar receiving systems is the ability to operate in the presence of interfering signals. One technique that has been shown to be capable of providing a margin of 30 or more dB against interference is the use of an adaptive antenna array. Adaptive arrays resemble conventional deterministically steered arrays in many respects. Each element has a complex weight, and the weighted element outputs are summed in an electronic summing element to obtain the array output. In the case of an adaptive array, however, the output is processed to derive control voltages that are fed back to the complex weights.

In this paper, we describe a type of compact adaptive antenna array that does not use an electronic summing element. This array, which we term a reactively steered adaptive array (RESAA), differs from other adaptive arrays fundamentally in that only a single element is connected by a transmission line to a receiver. The remaining elements are parasitic, and the pattern is formed according to the values of the reactive terminations on these parasitic elements. The array "summing" occurs in the currents on the one element connected to the receiver; thus, the electronic summing device and any associated mixers for processing at an intermediate frequency are not required.

This paper discusses experimental results and the theory for a RESAA consisting of five microstrip rectangular patch elements operating at a frequency of 4.0 GHz. Adaptive processing based on a steepest descent algorithm [1] is used to achieve closed loop control. Both a power inversion mode (nulling of an incident signal without a reference) and a mode that uses a synchronous reference to separate a desired signal from an interferer are considered. We find that a null with a depth of 30 dB (relative to the pattern maximum) and a width of about 25° can be steered toward an interferer. Typically, about 40 steps (iterations) are needed for forming the null; with the slow general purpose minicomputer that served as the controller (with programming in Fortran), adaptation times of several seconds were achieved.

Although microstrip patch elements were used here because of interest in a conformal array application, a RESAA can be fabricated with virtually any type of antenna element. Some early work on this technique has been reported [2], [3], [4] at several conferences, including applications at frequencies in the 10 to 30 MHz range using monopole elements.

After describing the theory of Harrington [5] and deriving an equation for the antenna pattern in terms of the reactive terminations and array configuration, we discuss the results of computer simulations of adaptive array behavior. From these simulations we developed an algorithm that was used with an experimental microstrip patch array; we conclude with a discussion of the experimental measurements with this array.

II. REACTIVELY STEERED ARRAY THEORY

Fig. 1 is a diagram of an array consisting of one element connected by a transmission line to a receiver and a set of closely-coupled parasitic elements, each terminated in a variable reactance. Harrington [5] first presented the theory for the pattern of such an array assuming (wire) dipole antennas, and then later [6] extended this theory to an array of dielectrically loaded waveguide-fed slot antennas. His analysis treated the array deterministically in the sense that reactive load selection was accomplished by an open loop technique. In this section, we review Harrington's analysis and apply it to the microstrip array.

Array Pattern for a General Parasitic Array

The analysis for a wire dipole array [5] begins using the Thevenin equivalent circuit of Fig. 2, which shows a load network and an N-port antenna system connected in parallel with series driving voltages. The terminal equation for the load and antenna system of Fig. 2 is

$$\vec{V}^{oc} = [Z_A + Z_L]\vec{I} \tag{1}$$

where $\vec{V}^{oc}$ and $\vec{I}$ are the column vectors of the Thevenin equivalent voltages and port currents, respectively. The matrices $[Z_A]$ and $[Z_L]$ are the open circuit impedance matrices of the antenna system and load system, respectively. Our interest is in the E_z component of the field radiated by the antenna array (see Fig. 1). By superposition, the electric field E_z radiated by the antenna

Manuscript received August 26, 1983; revised March 19, 1984.

The author is with the Michelson Laboratory. RF and Microwave Technology Branch, Naval Weapons Center, China Lake, CA 93555.

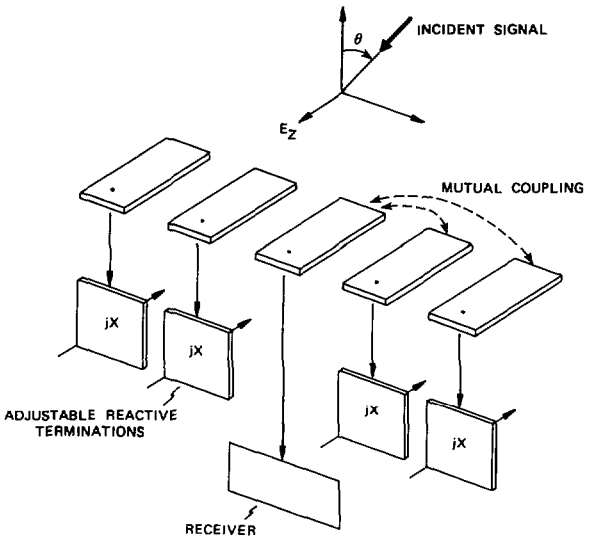

Fig. 1. Diagram of reactively steered array. Pictured elements represent the microstrip patches of the experimental array (minus the ground plane). Geometry for the pattern measurements is also shown.

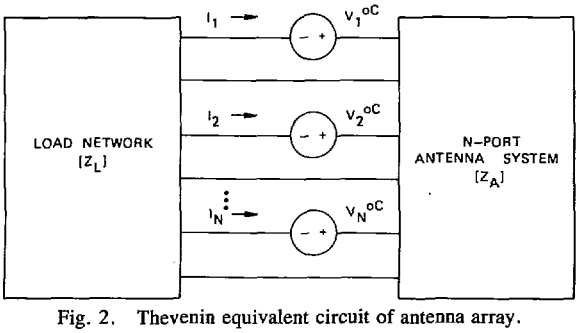

Fig. 2. Thevenin equivalent circuit of antenna array.

system can be written as

$$E_z = \sum_{n=1}^{N} I_n (E_z^{oc})_n \tag{2}$$

where $(E_z^{oc})_n$ is the field radiated when a unit current exists at port n, and all other ports are open circuited (oc). Equation (1) can be inverted, solved for $\vec{I}$, and substituted into (2) to give

$$E_z = \tilde{\vec{E}}_z^{oc} [Z_A + Z_L]^{-1} \vec{V}^{oc} \tag{3}$$

where $\tilde{\vec{E}}_z^{oc}$ is a row vector of the $(E_z^{oc})_n$. Since only the center element denoted by $p = (\overrightarrow{N+1})/2$ is driven in this array, $\vec{V}^{oc}$ is a vector with all zeros except for the pth element. Hence, (3) can be written as

$$E_z = V_p \sum_{n=1}^{N} (E_z^{oc})_n \{[Z_A + Z_L]^{-1}\}_{np} \tag{4}$$

where $\{\cdots\}_{np}$ denotes the np element of the matrix $[Z_A + Z_L]^{-1}$, and V_p is the open circuit voltage at the center (driven) element. For a given type of antenna element and array geometry, (4) can be used to determine the (unnormalized) array pattern by computing the elements of $[Z_A]$ and $[Z_L]$ and substituting the appropriate form for $\vec{E}_n$.

Microstrip Parasitic Array Pattern

The use of N-port network theory clearly is suitable for wire antennas and lumped element loads and was used, for example, to synthesize antenna patterns at 20 MHz in [2]. The applicability of the theory to aperture antennas and transmission line loads is not obvious; however, Harrington and Mautz [7] have shown that N-port network theory can be used for aperture problems by dividing the analysis into two separate regions by using the equivalence principle. One region contains only the loads, and the other region is the half-space into which the array radiates. Two aperture impedance matrices are computed, one for each region, that are independent of each other. Luzwick and Harrington [6] used this approach to analyze a reactively steered array of dielectrically loaded waveguide-fed slot antennas and arrived, after a lengthy analysis, at an equation of the same form as (4) (actually, the admittance equation that is the dual of (4)). Therefore, without proceeding through a complete derivation starting from equivalent current sheets for the microstrip patch elements, we assert that (4) can be used directly to write down the array radiation pattern. The task then is to derive expressions for $[Z_L]$, the diagonal matrix of reactive terminations; for $[Z_A]$, the impedance matrix for the radiation half-space; and for $\vec{E}_n$, which we take as the radiated electric field of an isolated microstrip patch element. An assumption implicit in this approach is that the radiation patterns of the patch elements are identical. For the closely coupled elements in the RESAA this assumption is probably violated to some degree, but the conclusions of the analysis and simulations are not expected to be affected. The general agreement between the simulation results and the experimental data confirms this view.

Load Matrix $[Z_L]$: The load matrix is diagonal, with entries of the form $(Z_L)_{ii} = jX_i$, except that $(Z_L)_{pp} = 0$ for the driven element. In the computer calculations given below, the X_i are also used to represent the reactive loads as normalized to 50 Ω. The experimental array employed reflection phase shifters; the phase of the reflection coefficient ϕ is related to the load reactance by

$$X = Z_0 \tan \phi. \tag{5}$$

Mutual Impedance Matrix $[Z_A]$: Several techniques for computing the mutal impedance between microstrip patch antenna elements have been reported [8]-[11], all of which require considerable machine computation and none of which can be written down in convenient analytical form. The equations due to Krowne and Sindoris [11] are the most straightforward; however, their applicability is somewhat limited, since the equations are suitable only for very closely spaced elements. For design and analysis of arbitrary patch arrays, theoretical expressions for the mutual impedance over a wide range of array parameters are needed. The simulations presented below avoid the problem by using measured mutual impedance values obtained from the experimental antenna.

Radiation Field $\vec{E}_n$: We use a transmission line model of a microstrip patch element with the coordinate system shown in Fig. 1. To within a factor that is constant for all elements, the radiation pattern for E is given by [12]

$$(E_z)_n = \frac{2 \sin (k_0 h \cos \theta/2)}{k_0 h \cos \theta} \cos (k_0 L \cos \theta/2) e^{jk_0 x_n \cos \theta} \tag{6}$$

where h is the substrate thickness, L is the patch width, and

$k_0 = 2\pi/\lambda$. The array pattern can then be written as

$$F(\theta) = \frac{2 \sin (k_0 h \cos \theta/2)}{k_0 h \cos \theta} \cos (k_0 L \cos \theta/2) \sum_{n=1}^{N} \{[Z_A + Z_L]^{-1}\}_{np} e^{jk_0 x_n \cos \theta}. \quad (7)$$

By reciprocity (7) is also proportional to the array output voltage when the array is receiving a signal polarized in the E_z direction and incident at an angle θ. The output voltage for angles and polarizations not encompassed by (6) can be obtained by using the appropriate element pattern factor in (7).

The connection between a reactively steered array and a conventional fully driven array can be made by noting that (7) can be written in the standard form of a fully driven array as

$$F(\theta) = g_e(\theta) \sum_n I_n e^{jk_0 x_n \cos \theta} \quad (8)$$

in which $g_e(\theta)$ is the element pattern and the feed currents I_n are

$$I_n = \{[Z_A + Z_L]^{-1}\}_{np}. \quad (9)$$

By comparison, the feed currents of the conventional array are given simply by $I_n^{\text{conv}} = A_n = |A_n| e^{j\theta n}$, where A_n is the complex weight for the nth element. The most noticeable difference between the feed currents of the reactively steered array and the conventional array are the former's nonlinear relationship between current and controlled variable (the X_i), and the dependence of each of its currents on all of the controlled variables.

Array Output as a Function of Reactive Terminations

A useful way to visualize the operation of a RESAA is in terms of a "control" surface that, for an array of N elements, is a surface in N-dimensional space of the array output as a function of the $N-1$ reactive loads. For the power inversion mode that is used for the simulations in the next section, this surface is also a plot of the control error, so that we will use the term "error surface." In particular, for a three-element array this surface can be completely displayed in Cartesian three-dimensional space.

Figs. 3, 4, and 5 present examples of the error surface for a three-element microstrip RESAA. In these figures, (7) is plotted for an array with the following characteristics:

- a three-element array is assumed in which each element is identical to the elements in the experimental array discussed below;
- the element spacing is the same as for the experimental array;
- the values for $[Z_A]$ in (7) are the values measured for the three center elements of the experimental array.

For each error surface plot the angle of incidence of the interference is fixed, and (7) is plotted as a function of X_1/Z_0 and X_3/Z_0. The error surfaces for this three-element example show one well-defined global minimum that corresponds to those values of the reactive terminations that reduce the incident interference to its lowest value at the array output. The location of the minimum changes as the incidence angle changes; in Fig. 6, the trace of the minimum point on the $X_1 - X_3$ plane is shown. Simulations with a larger number of elements and the experimental measurements show that multiple minima can exist.

In the simulations that follow, the incident signal and interference are both assumed to be E_z components. Additionally, a noncoherent system with a square law detector is assumed, so that the array output is computed as $V = [EE^*]^{1/2}$.

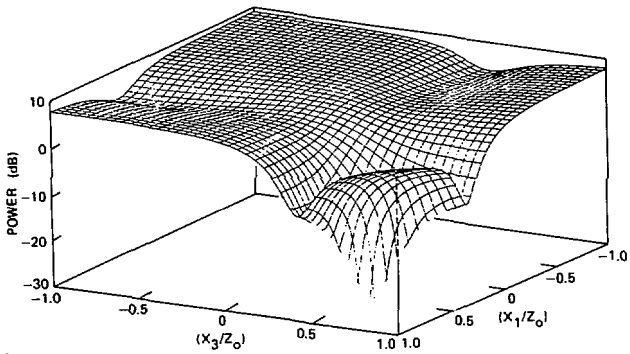

Fig. 3. Array output versus normalized reactive termination values for signal incident at $\theta = 0°$.

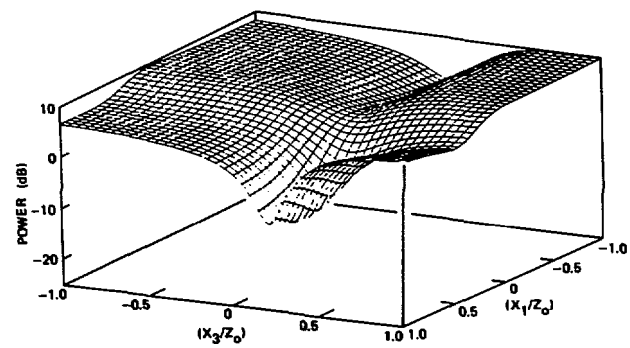

Fig. 4. Array output versus normalized reactive termination values for signal incident at $\theta = 45°$.

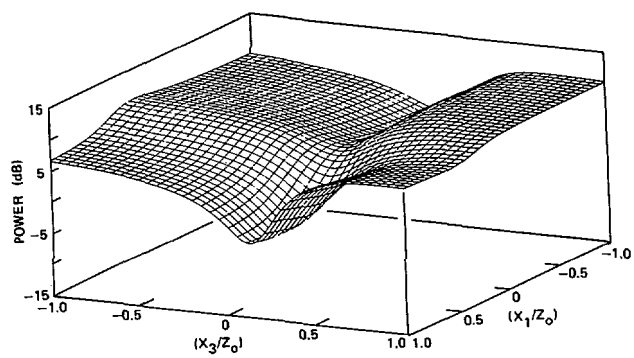

Fig. 5. Array output versus normalized reactive termination values for signal incident at $\theta = 90°$.

III. ADAPTIVE CONTROL SIMULATION

The adaptive control discussion and simulations were limited to a power inversion mode of operation for the array, in which the reactive loads are adjusted to minimize the output interference power without a reference signal. A discrete steepest descent method [1] was used to adjust the terminations.

Let $X_i(j)$ denote the reactive load on the ith antenna at the jth iteration. Then the discrete steepest descent algorithm states that the reactive load at the next iteration $X_i(j+1)$ is given by

$$X_i(j+1) = X_i(j) - K \nabla_x \epsilon \quad (10)$$

where K is a constant that controls the convergence rate, and ϵ

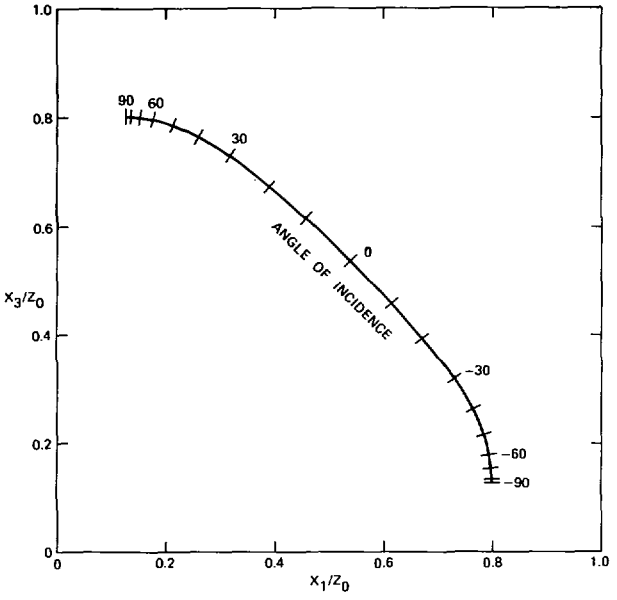

Fig. 6. Location of minimum in error surface as function of signal angle of incidence.

is the N-dimensional error surface. In terms of the error surfaces given in Figs. 3-5, the reactive loads are adjusted to follow a path that traces out the maximum value of the gradient at every point and that proceeds to successively lower values of the array output.

In a practical implementation of steepest descent control, the partial derivative in (10) can be measured by several different approaches. One analog approach is to superimpose a modulation signal ΔX on the reactive load control voltage and detect the corresponding change ΔR in the receiver output; the partial derivative is approximated by $\Delta R/\Delta X$. Since the partial derivative is needed for each parasitic element, either frequency or time multiplexing must be used to separate the responses at the receiver output for each element. For the experimental array described below, we used a digital approach to increment the terminations by a small value and then measure the resulting change in receiver output.

Simulation Results

The steepest descent algorithm was simulated on a HP-1000 computer. To generate the estimate of the error surface slope for (10), the change in the array output in response to a small change in each reactive termination was determined at each iteration. The small change in the reactive termination is referred to as the step size below.

Figs. 7 and 8 plot the evolution of the reactive loads X_1 and X_3 during the steepest descent algorithm for two different interference angles of incident. In both figures, the initial values of the normalized reactive loads are taken as 0.2, and curves for two values of K are shown.

In Fig. 9, the reduction in the interference power during convergence to the error surface minimum is shown for the cases presented in Figs. 7 and 8. Fig. 10 is a display of convergence time (defined as the number of iterations needed to reach 90 percent of the final value of the reactive load) and the peak-to-peak oscillation amplitude of the steady state reactive load value plotted as a function of the value of K. In Figs. 11 and 12, we show the pattern history for the runs given in Figs. 7 and 8.

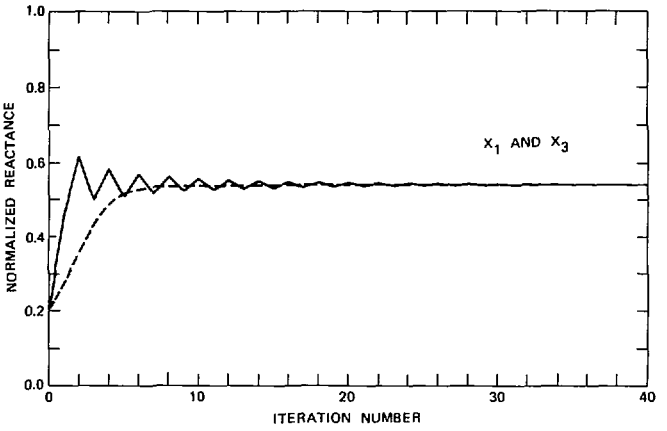

Fig. 7. Variation of reactive loads during steepest descent convergence on the error surface of Fig. 3. Interference incidence angle = 0°, step size = 0.01. For the dashed curve, K = 0.01; for the solid curve, K = 0.035.

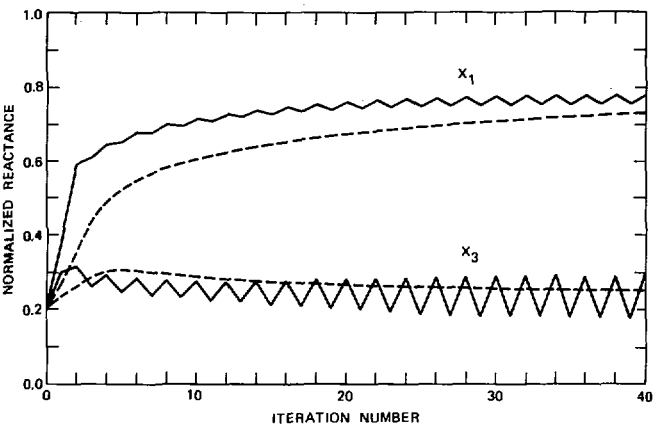

Fig. 8. Variation of reactive loads during steepest descent convergence on the error surface of Fig. 4. Interference incidence angle = −45°, step size = 0.01. For the dashed curves, K = 0.01; for the solid curves, K = 0.028.

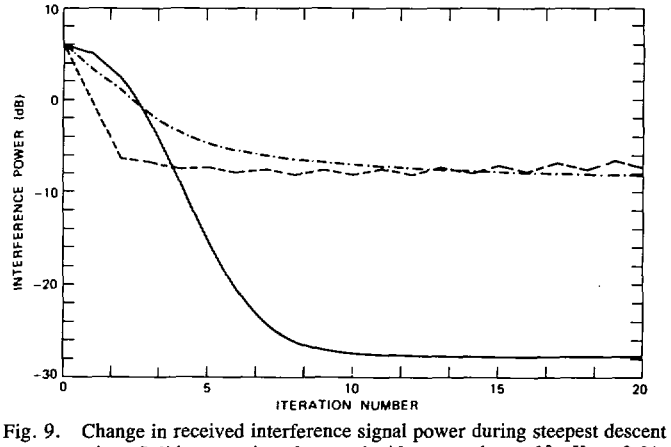

Fig. 9. Change in received interference signal power during steepest descent processing. Solid curve: interference incidence angle = 0°, K = 0.01. Dashed curve: interference angle = −45°, K = 0.028. Dot-dashed curve: interference incidence angle = −45°, K = 0.01.

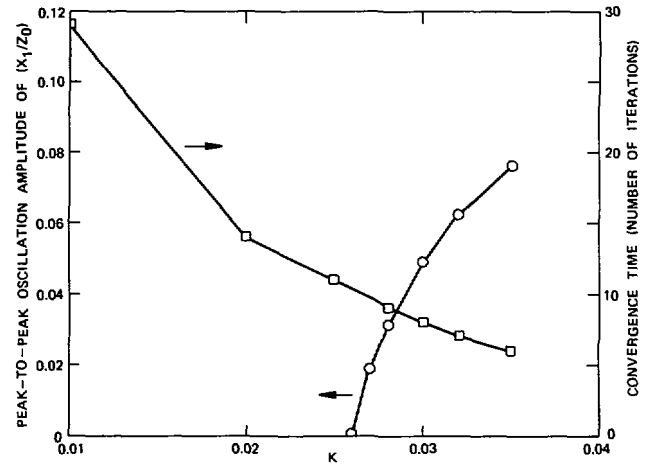

Fig. 10. Convergence time and steady-state reactive load jitter as a function of K. Interference incidence angle $= 0°$.

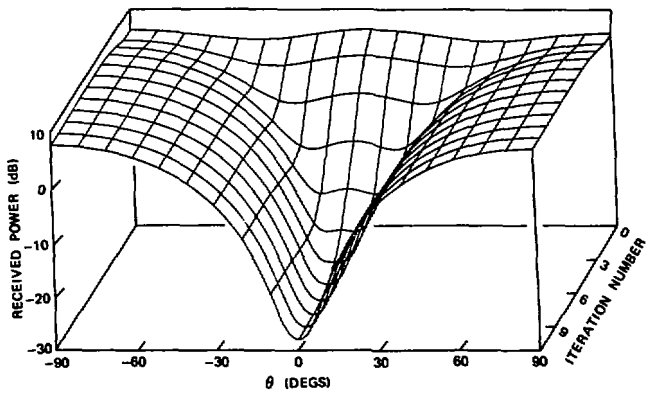

Fig. 11. Beam history during steepest descent processing for interference incident at 0°.

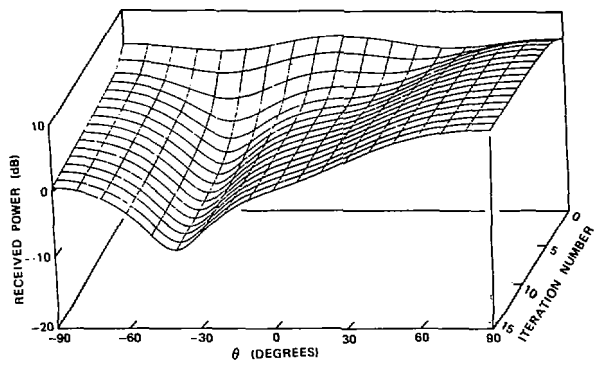

Fig. 12. Beam history during steepest descent processing for interference incident at $-45°$.

The following conclusions can be drawn from these curves (and from other curves not shown).

- The interference power reduction is greatest at broadside incidence (30 dB) and grows smaller toward endfire incidence (10 dB).
- The convergence time is fastest at broadside incidence and slowest at endfire incidence. The convergence time is related to the sharpness of the minimum (i.e., the second derivatives near the minimum); the sharper the minimum, the larger are the values of the gradient in (10) for fixed K. Figs. 3-5 show that the minimum is sharpest at broadside, which is consistent with the fast convergence.
- The noise from reactive load jitter resulting from "hunting" in the minimum is highest at endfire and lowest at broadside (for fixed value of K). Again, this is consistent with the shape of the error surfaces.
- A trade-off between convergence speed and steady state fluctuations in the reactive load values can be made. This kind of trade-off is usually required in adaptive antennas, and the reactively steered array is no exception.

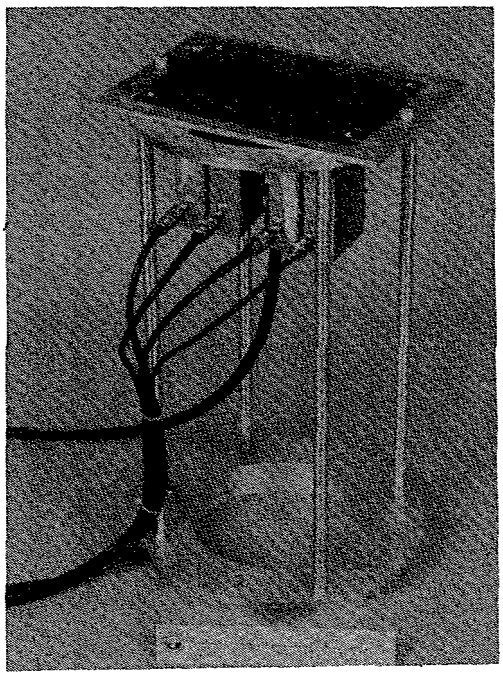

Fig. 13. Experimental antenna array. Scale in inches.

The control characteristics observed in the simulations were in general also observed in the experimental measurements described in the next section.

IV. EXPERIMENTAL RESULTS

Array Design

The experimental array, shown in Fig. 13, consisted of five microstrip rectangular patch elements. Each element measured 1.0 by 2.33 cm and was resonant at 4.0 GHz. The edge-to-edge separation was 0.75 cm, corresponding to a separation of 0.1 λ at 4.0 GHz. The experimental coupling results of Jedlicka *et al.* [13], along with extrapolation of our earlier experience [2] with arrays at 20 MHz, indicated that this separation would produce a sufficient amount of mutual coupling between elements. The substrate material was Rexolite 1422 with a thickness of 1.58 mm.

Reactive Load Design

A variable reflection phase shifter terminating a transmission line with a characteristic impedance Z_0 produces a variable reactance X given by $X = Z_0 \tan \phi$, where ϕ is the phase shift. Microstrip phase shifters were designed and fabricated to provide the necessary amount of phase shift, using a varactor diode mounted between a 50-Ω microstrip line and the ground plane. Approximately 250° of phase shift could be obtained with a bias voltage range of 0 to -10 V.

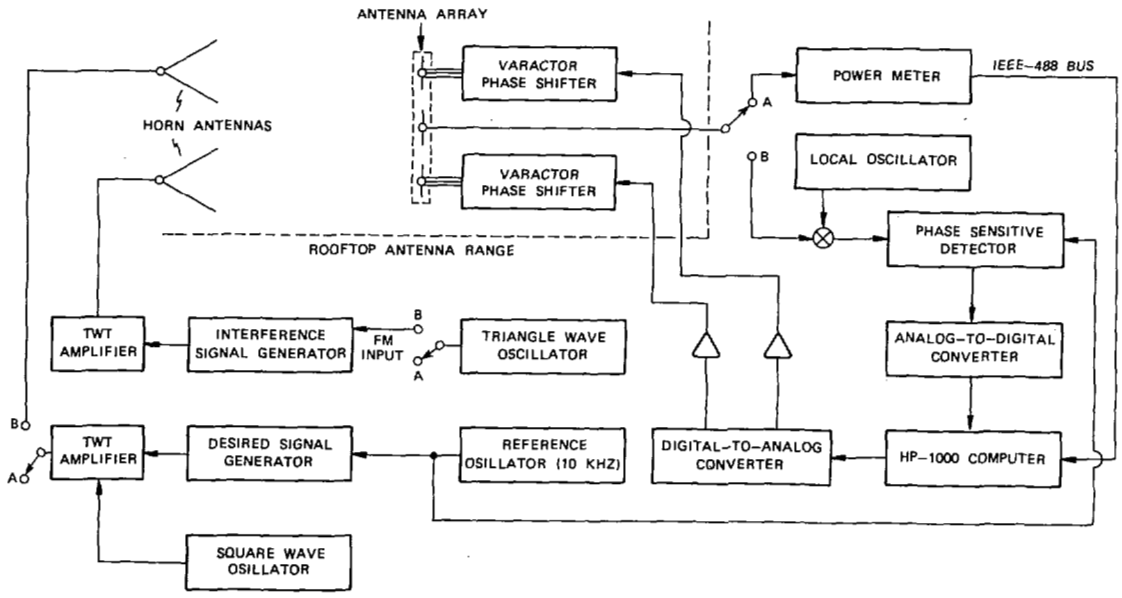

Fig. 14. Diagram of test setup.

Closed Loop Controller and Test Configuration

In Fig. 14 we show the array configured for closed loop operation on a rooftop test range. Two distinct operating modes are incorporated in this diagram. With the switches in position A, a power inversion mode (i.e., no reference signal) results; a digital power meter measured the array output and transferred the reading to a Hewlett-Packard HP-1000 computer over an IEEE-488 bus. For most of the measurements in the power inversion mode, only one source radiated, as Fig. 14 indicates. With the switches in position B, a reference mode results, in which a narrow band coherent receiver is modeled using a lock-in detector and a reference signal applied both to the lock-in detector and one of the radiating sources (the desired signal). A second radiating source represents an FM interference signal. In this reference mode the input signal to the computer was obtained from a fast analog-to-digital conversion (20 kHz conversion rate) of the lock-in output voltage. In both modes of operation, the control signals generated by the computer were converted to analog voltages with a range of 0 to -10 V and applied to the varactor bias port of the phase shifters. For the power inversion mode, the speed of the control loop was dominated by the slow transfer rate of the IEEE-488 bus; the results are presented in terms of the number of iterations, rather than absolute times. The reference mode was substantially faster because the IEEE-488 bus was not used.

Power Inversion Results

The control algorithm, written in Fortran on the HP-1000 computer, was a straightforward implementation of the steepest descent method used in the simulations. Rather than make a true measurement of all components of the gradient, however, at each iteration only one of the reactive loads was incremented by a small amount (referred to as the step size, below) and the change noted in the array output. If the array output was lowered, the next load was incremented and the array output measured, and so on sequentially and repeatedly through all of the terminations. When an incremental change produced an increase in the array output, the sign of the load increment was changed. We made numerous runs to investigate the effects of signal incidence angle, step size, feedback constant K, and termination initial values.

In Figs. 15-22 we show a selection of typical results. For all of these curves we have used a value of $K = 0.10$ v^2/mW (the units take this form because the reactive loads are controlled by the bias voltage and not by any measure of the load reactance). We found this value to be a good compromise between excessive steady state fluctuations and a convergence that was too slow.

For Fig. 15 we positioned the array so that the signal was incident at $\theta = 0^\circ$ (broadside) and set the initial values (V_0) of the terminations to either -4.0 or -2.0 V. The time history of the decrease in array output is shown; for initial values of -4.0 V, about 40 iterations are needed to decrease the power from the initial -20 dBm to a final value of about -55 dBm. At the nulling point the fluctuation in array output is about 10 dB, a typical result. For initial values of -2.0 V, the nulling is substantially poorer, with only about a 15 dB decrease in the array output realized. Apparently, initial values of -2.0 V cause the reactive loads to converge to a point that is substantially suboptimum. In general, we found that an initial point of -4.0 V for all terminations guaranteed a signal reduction of at least 30 dB for incidence angles of 45° to -45°, usually within about 40 iterations.

Fig. 16 displays the variation of the terminations during the -4.0 V curve of Fig. 15. The step size of 0.1 V and the method of sequentially testing for a decrease in array output are evident in these curves. The approach to a steady state value for each termination and a small "wander" in the steady state value can also be seen.

Another approach to selecting the initial point uses a random search phase. In this scheme, termination values are selected by a uniform random number generator, and the values producing the lowest array output at the end of the random search phase are entered as the initial values for the steepest descent algorithm. In Fig. 17 we show a power reduction curve in which a 10-step random search phase is followed by steepest descent processing. For this example the total number of steps to decrease the power from -20 dBm to -50 dBm is about one-half the number

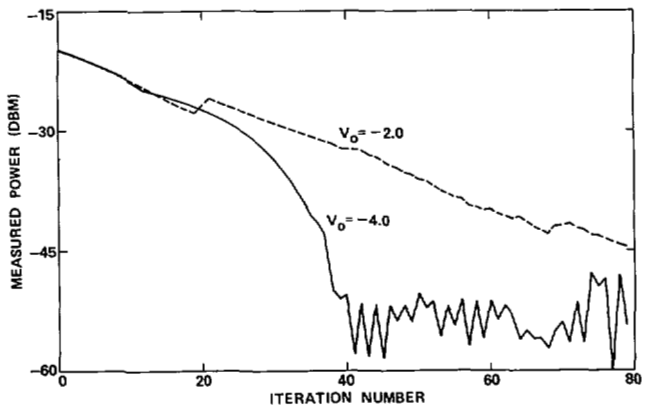

Fig. 15. Variation of array output power during nulling of signal incident at $\theta = 0°$. Curves for two different initial reactive load values are shown.

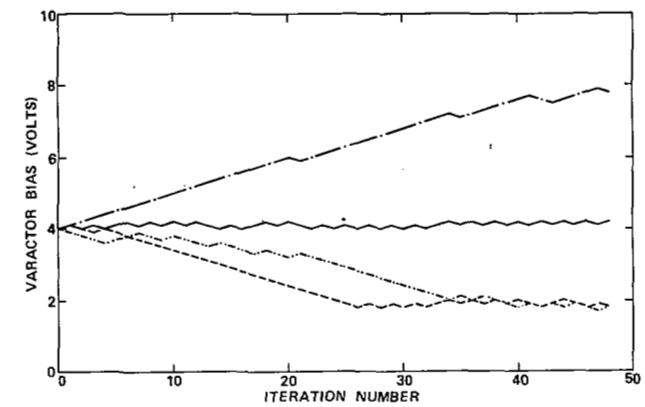

Fig. 16. Variation of the four reactive terminations during the signal nulling shown in Fig. 15 for $V_0 = -4.0$ V.

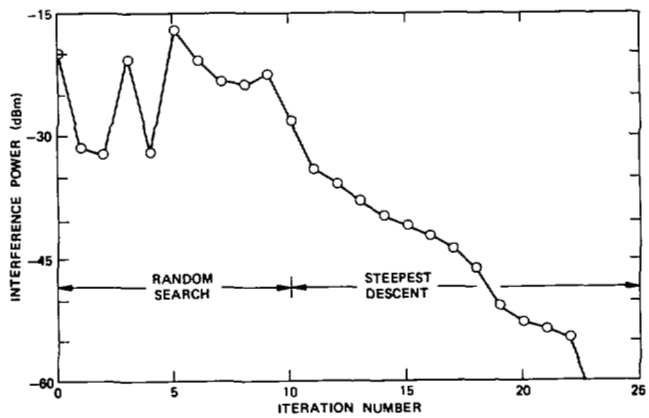

Fig. 17. Nulling produced by random search followed by steepest descent processing.

required when starting with −4.0 V on all terminations (Fig. 15); we have also found that the use of a random search phase usually produces a deeper null with smaller steady state flunctuations.

In Figs. 18 and 19 we plot typical antenna radiation patterns, showing the formation of a null toward the interference signal. Fig. 18 includes three traces to demonstrate that although the termination values necessary to produce a null in a given direction are not unique (i.e., multiple local minima occur in the error surfaces), the radiation patterns for all the possible solutions are remarkably similar. Three radiation patterns produced by the three sets of termination values that null a broadside signal are

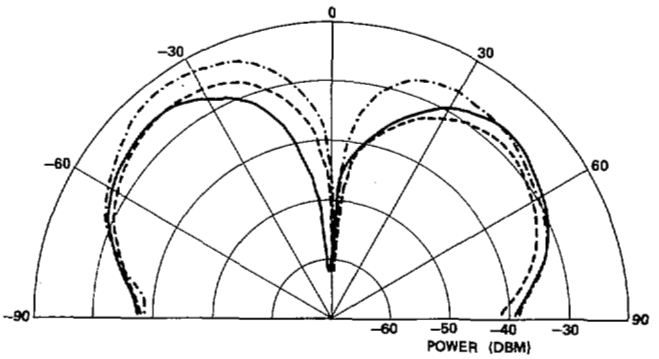

Fig. 18. E-plane antenna patterns for interference incident at $\theta = 0°$ resulting after nulling. The three patterns shown are produced by the three sets of reactive termination values listed in Table I. A power level of −20 dBm corresponds to 7 dBi.

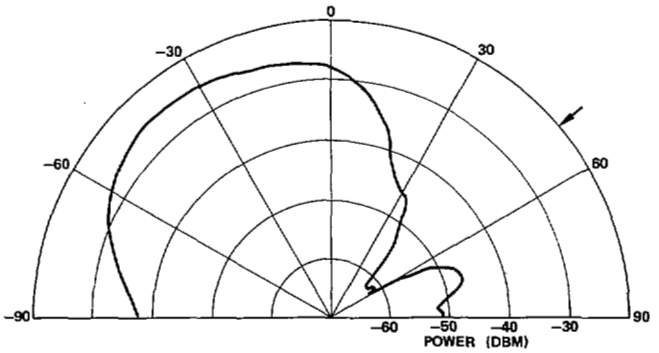

Fig. 19. E-plane antenna pattern for interference incident from angle indicated by arrow after nulling. A power level of −20 dBm corresponds to 7 dBi.

TABLE I
VALUES OF THE REACTIVE LOAD BIAS VOLTAGE (IN VOLTS) FOR THE THREE CURVES SHOWN IN FIG. 18

	Curve A (solid)	Curve B (dashed)	Curve C (dot-dashed)
Element 1	-0.16	-9.28	-3.68
Element 2	-5.96	-8.51	-6.55
Element 4	-3.53	-4.05	-0.69
Element 5	-5.56	-7.13	-5.83

Element 3 is the center element connected to the receiver.

shown; the termination values, which are listed in Table I, were arrived at by starting with different initial values.

In Fig. 20 we give an example of the frequency response of the array. The signal was nulled at a frequency of 4.0 GHz, the termination values were held constant, and the source frequency was then swept. Defining the nulling bandwidth as the frequency interval over which the null is at least 20 dB below the pattern maximum, a value of about 20 MHz is obtained for this array.

The effects of antenna rotation and source movement are displayed in Fig. 21. Following the initial nulling of the signal, during which time the antenna was stationary, the antenna was rotated at a rate of one degree for each three iteration steps. The null was tracked over a range of about 40°, at which point a noticeable increase in array output occurs. Comparison with Fig. 22, which plots the variation in termination values during the rotation of the antenna, shows that the array output increases

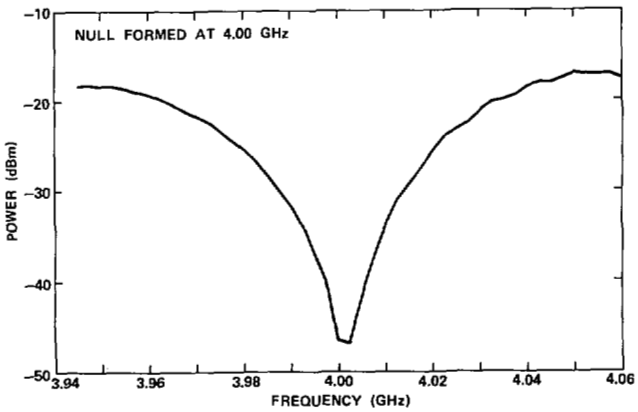

Fig. 20. Frequency response of null for interference incident at $\theta = 0°$.

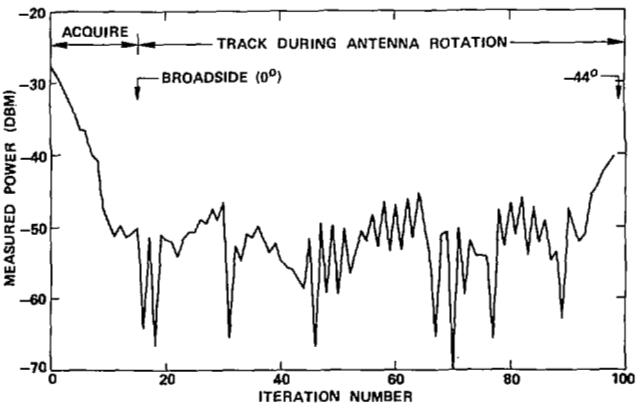

Fig. 21. Power received during nulling followed by antenna rotation.

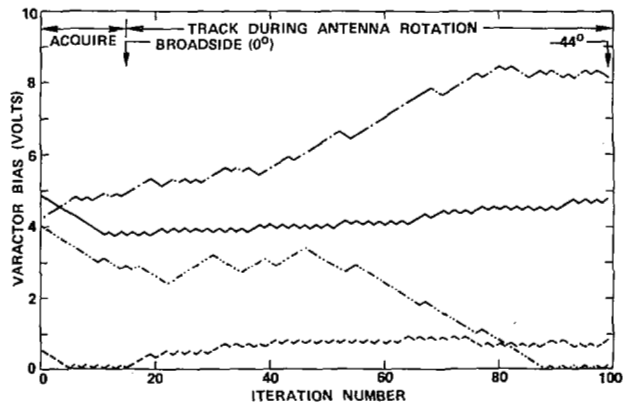

Fig. 22. Variation of reactive terminations during sequence given in Fig. 21.

because one of the terminations hits the limit at 0.0 V. Sometimes such a limit can be compensated for by changes in the other terminations (as, for example, occurred near iteration number 10), but in this particular case compensation did not occur. We have found that a random search phase leads to an initial null that can be tracked over a larger angular change than a null achieved after a start from a uniform set of values.

Reference Mode Results

An FM interference source, whose modulation bandwidth was centered about the 4.0 GHz center frequency of the array, radiated a power that was 20 dB higher than the desired signal (see Fig. 12). This interference was sufficient to prevent the lock-in detector from acquiring the desired signal. Fig. 23 shows a time history of the array output before adaptation, showing large impulses that occur when the FM source sweeps through the lock-in detector frequency.

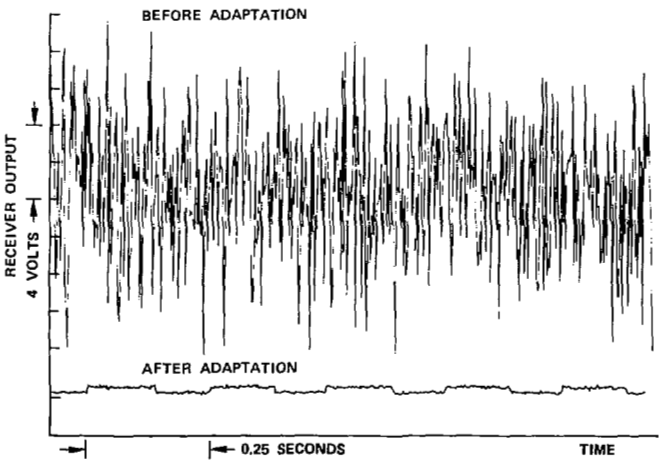

Fig. 23. Time traces of array output.

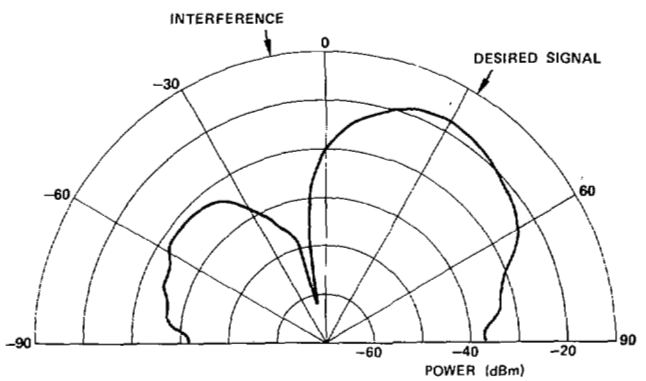

Fig. 24. *E*-plane antenna pattern following interference nulling and lobe steering toward a desired signal for time traces given in Fig. 23.

The adaptive algorithm used the same steepest descent technique described for the power inversion mode, except that the ratio of the second moment to the average value of the lock-in detector output was minimized. Minimization of this ratio placed a spatial null toward any signal producing an impulsive output and maintained a large pattern value toward any signal that was, by comparison, relatively smooth in its time variation. The post-adaptation trace in Fig. 23 and the pattern in Fig. 24 show the effect of the adaptive processing. A null was steered toward the FM interference souce, and a pattern maximum was maintained toward the desired signal. As indicated in Fig. 23, the square wave modulation on the desired signal was recovered.

V. DISCUSSION AND CONCLUSION

The results reported here demonstrate that a useful degree of pattern control of a microstrip adaptive array can be achieved by adjustment of the reactive loads on parasitic elements. Nulls with a depth greater than 30 dB and a width of about 25° were steered towards an interference source, with minimal distortion of the pattern towards other directions. The pattern was also controlled using a reference to generate a lobe toward a desired signal and a null toward an interference source. A reference signal must be provided by any of the methods described in the

literature; the books by Hudson [14], and Monzingo and Miller [15] discuss these methods.

The experimental measurements used a general purpose minicomputer with Fortran programming and a slow power measurement device, so that actual elapsed beamforming times were very slow. An estimate of the convergence time that could be achieved by a microprocessor controller can be made by assuming that the microprocessor cycle time (i.e., a fetch/operation/store cycle) is the limiting factor, rather than the analog-to-digital and digital-to-analog conversion speeds, or the response times of the receiver and reactive loads. Taking an average cycle time of 5 μs as typical of a fast microprocessor with coprocessor, estimating that each iteration step can be programmed with eight instructions, and taking 40 iterations as typical for convergence, a beamforming time of 1.6 ms results. Questions relating to stability of the algorithm at these rates are of course yet to be answered.

The main advantage of a RESAA, as compared with a conventional adaptive array, is the elimination of the mixers and other hardware needed to perform the complex weighting of each element's output at an intermediate frequency. In general, a RESAA configuration can be made with substantially fewer components than a comparable conventional adaptive array. It also lends itself (with microstrip elements) to fabrication as an integrated antenna, in which the phase shifter reactive loads are incorporated directly into a multilayered sandwich construction.

Another probable advantage is better pattern control (e.g., deeper nulls) for small element spacings. Gupta and Ksienski [16] have shown that least mean square (LMS) and Applebaum-type adaptive arrays can suffer in performance when element spacings are small because of mutual coupling effects. Although a direct comparison of the results in [16] and the results in this paper cannot be made because of somewhat different array configurations and assumptions, it appears that the amount of degradation in the signal-to-interference-plus-noise ratio for small spacings (one-quarter wavelength and less) is significantly less for the RESAA as compared with fully driven LMS and Applebaum-type adaptive arrays. An analysis that permits direct comparison between the RESAA and the results of [16] is currently in progress.

There are some disadvantages to the RESAA technique. Less control of the pattern is obtainable for the same number of elements, since only one control device is used for each element with the RESAA compared to the two control devices (for full complex weighting) for each element of a conventional adaptive array. Increased control over the pattern cannot be achieved simply by adding more elements, since new elements added at the periphery of the array have a progressively smaller mutual coupling with the receiving element and hence have progressively less influence on the pattern. And the control algorithm is somewhat more complicated than, for example, the LMS algorithm.

REFERENCES

[1] G. A. Bekey and W. J. Karplus, *Hybrid Computation.* New York: Wiley, 1968, pp. 270–280.

[2] R. J. Dinger and W. D. Meyers, "A compact reactively steered antenna array," in *1980 Antennas Propagat. Soc. Symp. Digest,* PQ, Canada, June 2–6, 1980, pp. 312–315.

[3] R. J. Dinger, "Adaptive microstrip antenna array using reactively terminated parasitic elements," in *1982 Antennas Propagat. Soc. Symp. Digest,* Albuquerque, NM, May 24–28, 1982, pp. 300–303.

[4] ——, "A microstrip power inversion array using parasitic elements," in *1983 Antennas Propagat. Soc. Symp. Digest,* Houston, TX, May 23–26, 1983, pp. 191–194.

[5] R. F. Harrington, "Reactively controlled directive arrays," *IEEE Trans. Antennas Propagat.,* vol. AP-26, pp. 390–397, May 1978.

[6] J. Luzwick and R. F. Harrington, "A reactively loaded aperture antenna array," *IEEE Trans. Antennas Propagat.,* vol. AP-26, pp. 870–873, July 1978.

[7] R. F. Harrington and J. R. Mautz, "A generalized network formulation for aperture problems," *IEEE Trans. Antennas Propagat.,* vol. AP-24, Nov. 1976.

[8] M. Malkomes, "Mutual coupling between microstrip patch antennas," *Electron. Lett.,* vol. 18, pp. 520–521, June 1982.

[9] T. M. Habashy, S. M. Ali, and J. A. Kong, "Impedance parameters and radiation pattern of two coupled circular microstrip disk antennas," *J. Appl. Phys.,* vol. 54, no. 2, pp. 493–506, 1983.

[10] C. M. Krowne, "*E*-plane coupling between two rectangular microstrip antennas," *Electron. Lett.,* vol. 16, pp. 635–636, July 1980.

[11] C. M. Krowne and A. R. Sindoris, "*H*-plane coupling between rectangular microstrip antennas," *Electron. Lett.,* vol. 16, pp. 211–213, Mar. 1980.

[12] R. E. Munson, "Conformal microstrip antennas and microstrip phased arrays," *IEEE Trans. Antennas Propagat.,* vol. AP-22, pp. 74–78, 1974.

[13] R. P. Jedlicka, M. T. Poe, and K. R Carver, "Measured mutual coupling between microstrip antennas," *IEEE Trans. Antennas Propagat.,* vol. AP-29, pp. 147–149, Jan. 1981.

[14] J. E. Hudson, *Adaptive Array Principles.* London: Institution of Electrical Engineers, 1981, p. 69.

[15] R. A. Monzingo and T. W. Miller, *Introduction to Adaptive Arrays.* New York: Wiley, 1980, pp. 175–176.

[16] I. J. Gupta and A. A. Ksienski, "Effect of mutual coupling on the performance of adaptive arrays," *IEEE Trans. Antennas Propagat.,* vol. AP-31, no. 5, pp. 785–791, Sept. 1983.

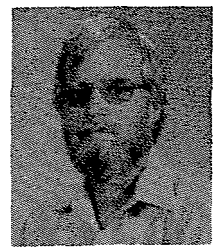

Robert J. Dinger was born in Washington, DC, on August 7, 1943. He received the Ph.D. degree in physics from the University of California, Riverside, in 1971.

Upon graduation, he joined the Research Department at the Naval Weapons Center, China Lake, CA, working in the area of millimeter wave nonreciprocal devices and superconducting magnetometers. In 1974, he accepted a position with the Naval Research Laboratory (NRL), Washington, DC in the Communication Sciences Division. From 1974 to 1981, he conducted research at NRL successively in the areas of cryogenic receivers for ELF submarine communications, noise and propagation in the lower VLF band, the spatial coherence of atmospheric noise in the ULF and ELF bands, and compact high frequency adaptive arrays. In 1981, he returned to the Naval Weapons Center (NWC) as the Head of the RF and Microwave Technology Branch in the Research Department. His current interests at NWC include adaptive array processing, radar glint reduction using polarization diversity, and radar target classification and identification. He is an Extension Lecturer for the Electrical Engineering Department of the California State University, Northridge.